

Learning Physics From Video: Unsupervised Physical Parameter Estimation for Continuous Dynamical Systems

Alejandro Castañeda Garcia
Delft University of Technology
m.a.castanedagarcia@tudelft.nl

Daan Brinks
Delft University of Technology
d.brinks@tudelft.nl

Jan van Gemert
Delft University of Technology
j.c.vangemert@tudelft.nl

Nergis Tömen
Delft University of Technology
n.tomen@tudelft.nl

Abstract

Extracting physical dynamical system parameters from videos is of great interest to applications in natural science and technology. The state-of-the-art in automatic parameter estimation from video is addressed by training supervised deep networks on large datasets. Such datasets require labels, which are difficult to acquire. While some unsupervised techniques –which depend on frame prediction– exist, they suffer from long training times, instability under different initializations, and are limited to hand-picked motion problems. In this work, we propose a method to estimate the physical parameters of any known, continuous governing equation from single videos; our solution is suitable for different dynamical systems beyond motion and is robust to initialization compared to previous approaches. Moreover, we remove the need for frame prediction by implementing a KL-divergence-based loss function in the latent space, which avoids convergence to trivial solutions and reduces model size and compute.

1. Introduction

Estimating dynamical parameters of physical and biological systems from videos allows relating visual data to known governing equations which can be used to make predictions, improve mathematical models, understand diseases, and, in general, advance our knowledge in science and technology [6, 18, 32]. Use cases include trajectory prediction for celestial objects [15], healthy and diseased tissue characterization [14], and physical model validation [6, 7].

Fitting governing equations is an inverse problem [2], which often requires either using additional sensors to directly measure system states. Instead, doing measurements from a video allows to avoid additional sensors, yet,

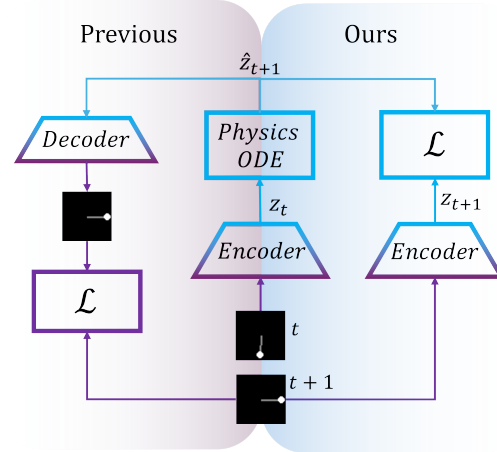


Figure 1. We propose a novel unsupervised approach to physical parameter estimation from videos. The black squared images are video frames with different states of a white pendulum. Starting from a frame at time t (center) parameter estimation techniques typically employ an encoder, which estimates the dynamical states z_t at time t . A physics block (Physics ODE), with learnable parameters, then solves the governing equations of the dynamical system to predict future dynamical states \hat{z}_{t+1} , which takes place in the latent representation (blue lines). Previous state-of-the-art methods (left) then design decoders to reconstruct the next frame at time $t + 1$ and use reconstruction loss (\mathcal{L} , purple left) to train the physics ODE block. In contrast, our method (right) completely avoids the need for a decoder by leveraging a loss function in the latent space (\mathcal{L} , right). Our loss (blue) function minimizes the distance between the estimated states \hat{z}_{t+1} and z_{t+1} .

requires manually labelling pixels or video frames which is time-consuming and expensive. Therefore, automated and unsupervised methods are needed to extract dynamics from videos and accurately estimate physical parameters [6, 15, 17, 18, 32].

Recent work addressed parameter estimation from video by deep learning [6, 7, 37] or reinforcement learning [3]. For instance, proposed supervised learning methods rely on datasets with extensive and high precision labels which are exceedingly difficult to obtain [1, 4, 26, 28, 35]. To avoid labeling, current unsupervised methods for estimating physical parameters build on encoder-decoder network designs: reconstructing video frames from low-dimensional representations. The frame reconstruction is a mere by-product of the parameter estimation, and leads to overly complex solutions which are difficult to train [15, 18]. Along with this, current solutions [15, 18, 20, 38, 43] are constrained to motion dynamics, excluding a wide variety of systems like dynamics related to brightness, colour, and deformations, among others [15, 18].

Our work proposes an unsupervised learning method to solve the inverse problem using videos of a dynamical system with known, continuous governing physics equations. Our method can be implemented for different dynamical systems beyond motion problems. Thus, unlike previous approaches, we present an evaluation of the latent space of our model in multiple dynamical systems. We show that our unsupervised model successfully fits the dynamics and effectively generalizes to unseen future frames. In addition, we bypass frame reconstruction by calculating the loss simply in the latent space, eliminating the need for a decoder. Our approach is thus fast, less resource-intensive and more robust to initial conditions compared to existing methods.

Our approach is visualised in Figure 1, and our main contributions are summarized as:

- Accurate dynamical state estimation from video with precise extrapolation at test time.
- Allowing inverse problems beyond motion, such as appearance and scaling.
- An unsupervised latent space loss to avoid expensive video frame reconstruction;
- Easy model training with robustness against different initial conditions.

Our code and datasets will be made available on GitHub.

2. Related Work

Physics and Deep Learning The relationship between physics and deep learning is symbiotic. Physics inspired segmentation [25] and generative models [33, 34] as well as the design of new architectures [12]. Likewise, deep learning is used to study, understand and create new physics from data [6, 7, 17, 37]. Techniques like physics-informed neural networks (PINN) [21, 31] or Lagrangian neural networks (LLN) [8, 27] are designed to solve inverse problems. Yet,

PINNs are usually constrained to initial conditions, boundary conditions, and time reference [11, 21, 29]. Moreover, these methods are supervised and require labeled data. Because obtaining labeled data in inverse problems is expensive or even infeasible [1] we avoid the need for labels and offer an unsupervised method, following [1, 4, 26, 28, 35]. Our work focuses on the the inverse problem of physical parameter estimation from video using unsupervised machine learning.

Learning Physics from Video Work on learning physics from recorded videos focus on frame prediction [5, 10, 13, 24] and do not concentrate on estimating physical parameters from video. Existing research on extracting physical information from video [40] estimates parameters such as the friction coefficient, or the value of the dynamical state variable such as the position or velocity. These methods are supervised and require labelled datasets with access to the dynamical variables or parameters’ ground truth [9, 27, 31, 37, 39–42]. Moreover, these methods mainly focus on motion problems and are based on systems similar to interaction networks [5, 36, 37]. Some methods [19, 38] aim to parameterize and solve differential equations to simulate the deformations. However, dynamical systems are not limited to motion, and we here propose a method that goes beyond motion which we illustrate with use-cases for appearance changes, and scaling.

Unsupervised Parameter Estimation from Video Existing unsupervised work use frame representation and prediction with physics priors of known governing equations with unknown parameters to estimate [15, 18, 20, 38, 43]. Some approaches [20, 43] use variational auto-encoders (VAE)[23] with a physics engine between the encoder and the decoder to estimate parameters; however, the reconstructions are poor, constraining the model to simple motion problems. The most similar work to ours are [15, 18] where they estimate parameters from a single video without annotations, and we experimentally compare against them. Our method is favourably compared in terms of robustness to initializations; we examine the latent space and extension to different dynamics.

Baselines As a strong, unsupervised parameter estimator, Jaques et al. [18] uses a traditional auto-encoder with a physics engine in the latent space to reconstruct inputs and generate future frame predictions. The model also incorporates a U-Net in the encoder to learn segmentation masks for the object of interest in an unsupervised way; the capability to learn this mask is linked to the spatial transformer (ST) they use in the decoder similar to [16]. During inference, the spatial transformer is used to perform affine transformations on the mask to ‘move’ the object in future frame predictions. This limits the application of [18] to affine motion dynamics.

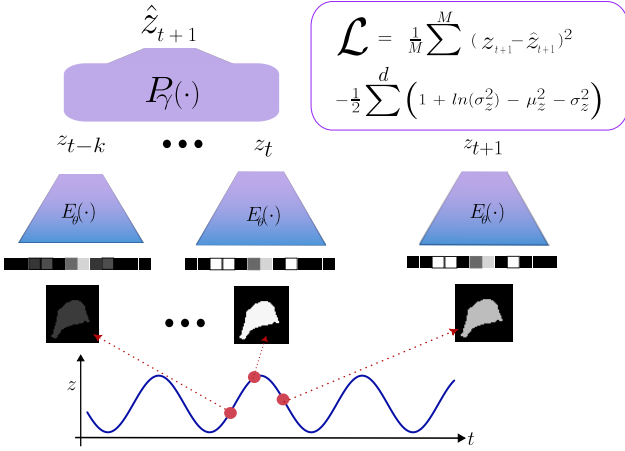


Figure 2. Method overview. A video recording of an object with a periodic brightness change (bottom) displays dynamics z_{real} with sampling period δt . Each frame is mapped by the encoder $E_\theta(\cdot)$ to the unsupervised latent representation z_t . The physics block $P_\gamma(\cdot)$ generates a prediction of the future step \hat{z}_{t+1} , which we compare to the encoded representation z_{t+1} of the corresponding frame. **Top-right:** Loss function of our model; the first term ensures the prediction fits with the encoding, while the second expression controls the variance of z .

On the other hand, Hofherr et al. [15] uses a differentiable ODE solver to estimate the parameters. This model also uses a spatial transformer, but at the pixel level, the object pixels are displaced using the prediction made by the ODE solver. The model needs to be trained, along with the use of masks, to learn which pixels should be translated. Finally, using frame reconstruction to achieve parameter estimation is challenging and makes the network slow to train since reconstructing frames from low dimensional data (i.e., a set of positions and velocities) is an ill-defined problem. Therefore, [15, 18, 38] had to limit their scope to using a mask and a spatial transformer [16], excluding dynamical systems with changes in intensity and colour, deformations and non-uniform scaling among others which we explicitly allow in our paper.

3. Methods

Our approach aims to estimate the parameters of a known governing equation from a video recording; since it is unsupervised, the training set consists of unannotated frames with a known frame rate denoted as δt . While existing methods which depend on frame prediction use complete auto-encoder architectures, our method is composed only of a simple encoder and a physics block. Figure 2 shows our approach altogether: first, the relation between the system dynamics and the frames; second, how the encoder processes the video frame by frame to obtain the latent space representation;

and finally, how our physics block makes predictions to be used in our unsupervised loss function.

Scope We study systems represented by autonomous differential equations since those models just depend of the state variable which is captured in video, and it is not affected by external forces and takes the form:

$$z^{(n)} + \gamma_{n-1}z^{(n-1)} + \dots + \gamma_1z^{(1)} + \gamma_0z = 0, \quad (1)$$

which is an n^{th} -order system, where z is the time-dependent state variable or "dynamic variable", $z^{(k)}$ with $k = 1, 2, \dots, n$ is the k^{th} -derivative of z with respect to time t and γ_i with $i = 0, 1, \dots, n-1$ are the parameters of the equation we want to estimate.

In the following *Proof-of-concept* we first consider a second-order differential equation:

$$z^{(2)} + \gamma_1z^{(1)} + \gamma_0z = 0. \quad (2)$$

Encoder: The encoder is a network $E_\theta(x)$ that maps images $x \in \mathbb{R}^{w \times h \times c}$ to the state variable $z \in \mathbb{R}^d$, where d is the number dynamic variables to study. We used an MLP with three layers and ReLU as an activation function for the mapping.

$$E : \mathbb{R}^{w \times h \times c} \rightarrow \mathbb{R}^d$$

$$z_t = E_\theta(x_t). \quad (3)$$

Physics block: Our physics block numerically solves the differential equation using Euler's method:

$$z_t^{(1)} \approx \frac{z_{t+1} - z_t}{\delta t} \approx \frac{z_t - z_{t-1}}{\delta t} \quad (4)$$

$$z_{t+1} = z_t + \delta t z_t^{(1)} \quad (5)$$

$$z_{t+1}^{(1)} = z_t^{(1)} + \delta t z_t^{(2)}. \quad (6)$$

Plugging in Eq. 2, we can rewrite the physics block as:

$$\hat{z}_{t+1} = z_t + \delta t \left(z_t^{(1)} - \delta t (\gamma_1 z_t^{(1)} + \gamma_0 z_t) \right) \quad (7)$$

$$P : \mathbb{R}^d \rightarrow \mathbb{R}^d$$

$$\hat{z}_{t+1} = P_\gamma(z_t, \dots, z_{t-n}; \gamma) \quad (8)$$

where γ_i are learnable parameters and the predicted latent space for time $t+1$ is a function $P_\gamma(\cdot)$ of the latent representations of the n previous frames. We use the notation \hat{z} for the latent space predicted using the function P , which is different from z predicted by the encoder.

Predictions: The encoder maps images $x_t \in \mathbb{R}^{w \times h \times c}$ to the state variable $z_t \in \mathbb{R}^d$ for all time steps $t \in [0, T]$

leading to \hat{z} with dimensionality $\mathbb{R}^{T \times d}$ for all input frames. In particular, we have the following two vectors:

$$\mathbf{z} = \begin{bmatrix} z_n \\ \vdots \\ z_{t+1} \\ \vdots \\ z_T \end{bmatrix} = \begin{bmatrix} E_\theta(x_n) \\ \vdots \\ E_\theta(x_{t+1}) \\ \vdots \\ E_\theta(z_T) \end{bmatrix} \quad (9)$$

$$\hat{\mathbf{z}} = \begin{bmatrix} \hat{z}_n \\ \vdots \\ \hat{z}_{t+1} \\ \vdots \\ \hat{z}_T \end{bmatrix} = \begin{bmatrix} P_\gamma(z_{n-1}, \dots, z_0; \gamma) \\ \vdots \\ P_\gamma(z_t, \dots, z_{t-n}; \gamma) \\ \vdots \\ P_\gamma(z_{T-1}, \dots, z_{T-n}; \gamma) \end{bmatrix} \quad (10)$$

Loss function: The first goal of the loss function is simply to minimize the difference between the predictions \mathbf{z} and $\hat{\mathbf{z}}$ over a batch of size M . Therefore, our loss function is given first by:

$$\mathcal{L}_1 = \frac{1}{M} \sum_{i=1}^M (z_i - \hat{z}_i)^2 = \frac{1}{M} \sum_{i=1}^M \left[E_\theta(x_i) - P_\gamma(E_\theta(x_{i-1}), \dots, E_\theta(x_{i-n})) \right]^2 \quad (11)$$

However, one problem with this approach is the convergence to the trivial solution such that $E_\theta(x) = 0 \forall x$ and $P_\gamma(z) = 0 \forall z$. To avoid this problem, we want to induce variance in the encoder’s output: we propose a variational latent space and assume $z_k \in \mathcal{N}(\mu, \sigma^2)$. The values of μ and σ^2 effectively define the range of z since this consists of a re-normalization of the metric. Based on the VAE approach [23], we define the second part of the loss function using the Kullback-Leibler divergence (KL-divergence). Thus, z_k is an element of the random variable $Z \sim \mathcal{N}(\mu_z, \sigma_z^2)$ and we want it to follow a particular distribution $Q \sim \mathcal{N}(0, 1)$, then KL-divergence is given by:

$$\mathcal{L}_2 = \text{KL}(Z||Q) = -\frac{1}{d} \sum_{i=1}^d (1 + \ln(\sigma_z^2) - \mu_z^2 - \sigma_z^2) \quad (12)$$

Here, the KL-divergence is used differently than conventional: VAEs [23] typically assume the encoder finds the correct distribution, and use the sampling trick to obtain the decoder input. In our proposal, we do not sample from the latent distribution. Instead, we constrain the encoder to learn the dynamical state variable. Thus, we calculate the mean μ_z and variance σ_z^2 over the batch in the loss.

Finally, combining the two loss functions:

$$\mathcal{L} = \mathcal{L}_1 + \mathcal{L}_2 = \frac{1}{M} \sum_{i=1}^M (z_i - \hat{z}_i)^2 - \frac{1}{d} \sum_{i=1}^d (1 + \ln(\sigma_z^2) - \mu_z^2 - \sigma_z^2) \quad (13)$$

Our loss function (Eq. 13) serves several purposes: First, $E_\theta(\cdot)$ maps images to random variables z in latent space, and L_2 guarantees that z is normally distributed. Then, the function $P_\gamma(\cdot)$ preserves the sense of order and relation between latent spaces from different frames. Since we are analyzing a single video, z contains information about the temporal properties of the sequence of frames. Finally, L_1 makes the model consistent since the physical predictions made by the physics block $P_\gamma(\cdot)$ are generated by $E_\theta(\cdot)$.

Training: For parameter estimation in the physics block $P_\gamma(\cdot)$, we used a learning rate proportional to the initial value γ_k^0 of the learnable parameter γ_k , where $\text{lr}_{(\gamma_k)} \sim 10^{[\log_{10} |(\gamma_k^0)|]}$. This approach provides sufficiently large step sizes at the beginning of training to escape of local minima. Further training details are in Appendix A.2.

4. Experiments

4.1. Fully controlled video datasets

We propose to find solutions to inverse problems that extend beyond simple video motion dynamics. Therefore, to evaluate three different continuous dynamical systems involving motion, intensity and scaling. We describe the details about dimensionality in Appendix. A.1.

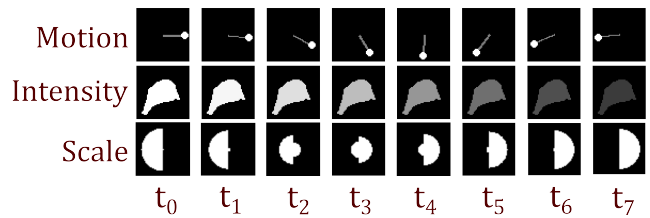


Figure 4. Example frames from our datasets. Each row shows a different dataset, corresponding to a different continuous dynamical system, and each column a different time sample.

Motion systems can be understood as problems where pixels have a translation or rotation transformation; classic examples include pendulums, springs, and celestial movements. For the motion system, we simulated a pendulum since the majority of related literature uses it as an example. In this dataset, the state variable is the angle of the pendulum $z_{real} = \theta \in [-90.0^\circ, 90.0^\circ]$.

Intensity dynamics consists of the change in grayscale pixel values. This problem can be seen in nature in voltage

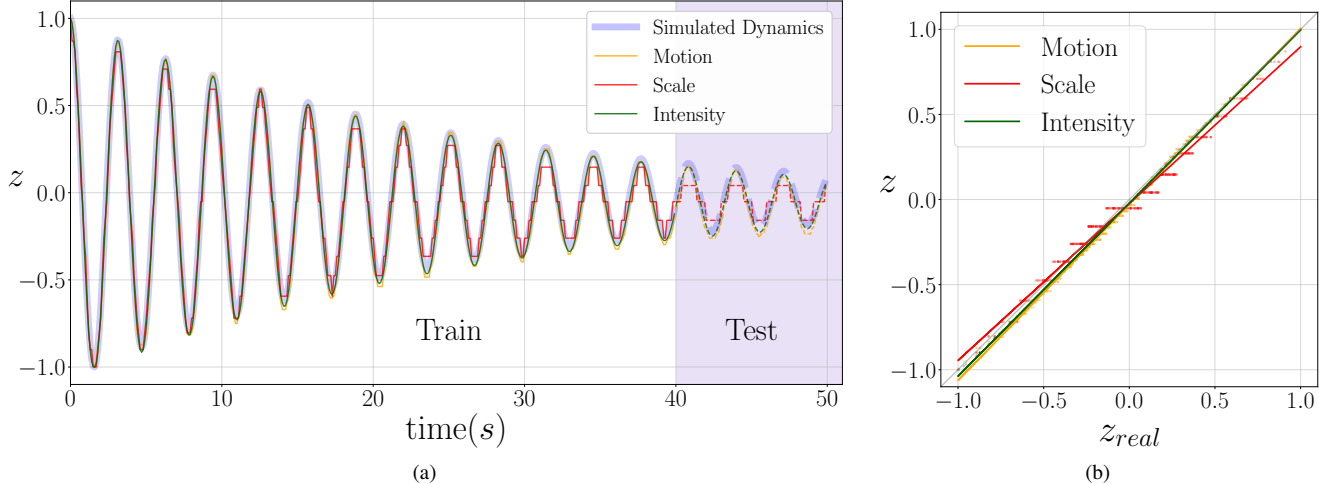


Figure 3. **(a)** Latent space estimation of the dynamic variable z for the three datasets. The blue line shows the ‘ground truth’ value z_{real} of the simulated dynamics, the model was trained with the dynamics of the continuous line while the dotted line is the predictions of the test set. **(b)** Encoder output z vs. z_{real} for every frame in (a). We find that our unsupervised loss leads to a good agreement between the predicted and ground truth dynamics.

imaging of spiking neurons or photonic crystals. To create this dataset, we generated an irregular shape and assigned all pixels inside the corresponding intensity of our dynamical system. We normalized the intensity dynamics to be in the range $z_{real} \in [0.2, 1.0]$.

Scale in a video refers to changes in the total number of pixels corresponding to our object of interest. It can be related to a growing bacteria population or liquid diffusion. For this dataset, we created a filled circle centred in the middle of the image, where the radius is proportional to the dynamic variable. However, the scaling transformation is not symmetric; while one half of the circle grows, the other half becomes smaller and vice versa. Here, we normalized the range of the radius dynamics between $z_{real} = r \in [-10, 10]$.

State-of-the-art methods are tested on simulated datasets like ours [9, 18, 36, 37, 41, 42], where the image consists in a fixed black background, while the individual objects in the scene are in different channels of the image, from now on we refer to this representation as a "mask". The pendulum system is a typical case of study, but for scale and intensity, there were no baselines available. In Figure 4, we illustrate the behaviour of the three different datasets.

4.2. Latent Space Evaluation

First, we train our model using the three synthetic datasets and evaluate the dynamics z estimated by the encoder $E_{\theta}(\cdot)$. We compare the estimated state variable z to its ground truth value z_{real} , which was used to generate the data. Following Eq. 2, we consider second-order dynamics for the three datasets, where the evolution of the state variable z follows

a dampened oscillation.

In Figure 3, we show that the model is capable of estimating the dynamics z for all three datasets. Although oscillatory dynamics can be challenging for neural networks, we find that our unsupervised loss fits the dynamical behaviour reasonably, with small deviations from the ground truth. Figure 3b depicts the encoder output z against the ‘ground truth’ dynamics z_{real} for every frame the train and test set (dots). For better visualization, a straight line (solid lines) was fitted to each dataset.

Importantly, our model output has complete physical interpretability since we directly use the differentiable, second-order ODE (Eq. 2) in the physics block during training. Due to these physics priors, the model is able to generalize at test time to frames at time steps unseen during training. The network’s extrapolation of z to unseen future time steps is shown using dashed lines in Figure 3a.

We observe that the most accurate results are obtained using the ‘Intensity’ dataset; this stems from the fact that the temporal information is in the pixel intensities instead of location, which means that in the intensity dataset, information about the dynamics is less discretized than the other datasets. Specifically, using 8-bit integer values for pixel intensities, the input can assume 256 different values. In contrast, with motion and scaling, the dynamics are discretized by the pixel locations. In particular, for a (50×50) frame size, the discretization of the dynamic variable is increasingly more impactful, especially as the oscillation amplitude is decreased. This effect is seen clearly in the latent space dynamics of the ‘Scale’ dataset

in Figure 3a (red line), which displays discrete jumps. The discretization error also disproportionately affects the parameter estimation in the ‘Scale’ dataset, specifically the prediction of the parameter γ_1 , which is discussed in the next section.

4.3. Parameter estimation Accuracy

In this section, we present the accuracy of the model in learning the parameters γ of the dynamical system equations. As in section 4.2, we consider second-order governing equations as defined in Eq. 1. We note that γ_0 is the frequency and γ_1 is the damping factor of the oscillations.

Table 1 shows the model’s accuracy to estimate γ . We used equation 2 to simulate the dynamics; details of the ground truth are given in Appendix. A.3. On the one hand, The results show the model is pretty accurate in calculating γ_0 ; this parameter defines the oscillation frequency of the system; in figure 3, we validate the model is accurate in finding it. On the other hand, γ_1 is the damping factor of the model; the three experiments present different performances. However, according to the discretization discussed in section 4.2, the inaccuracy in the motion and scale dataset is anticipated.

4.4. Robustness and Stability

While previous work can reliably generate frame reconstructions using physics blocks in latent space, they often lack an analysis of the parameter estimation. Thus, it is not known if the generated frames correctly use the latent space information in an interpretable manner. In fact, it is known that the models presented in baselines are sensitive to initialization and may fail to converge [15, 30]. In this section, we evaluate the robustness of our model against changes in parameter initializations.

We initialize the learnable parameters γ of Eq. 2 in the interval $[-10.0, 10.0]$ over multiple runs. The ground truth values used to generate the synthetic datasets were $\gamma_0 = 4$ and $\gamma = 0.08$. In Figure 5, we show the convergence of the parameter prediction during training with different initializations. As can be seen, the model converges close to the ground truth values for each dataset, independent of the initialization. The shaded area highlights that while the trajectories may initially diverge, the model is capable of finding the correct parameters consistently. Table 1 shows the final accuracy of this experiment.

4.5. Baseline comparison

In this section, we compare against the baselines PAIG [18] and NIRPI [15] discussed in Sec. 2. We did not use our datasets in the comparison since baselines are not designed to handle our intensity and scale setting. Therefore, for a fair

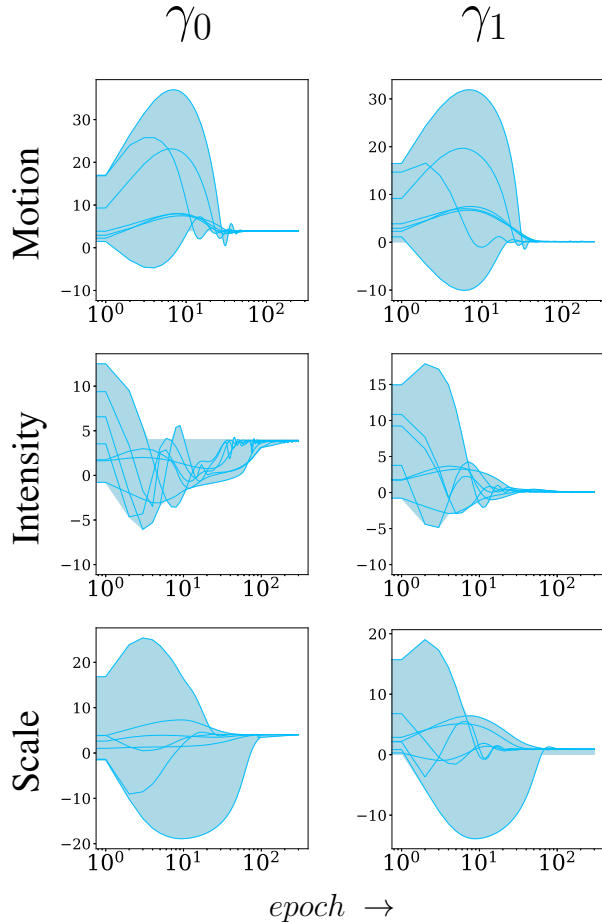


Figure 5. Robustness of the parameters estimation against different initializations. The rows indicate the different dynamical systems, while the columns are the parameters to estimate. The vertical axis corresponds to the parameter value, and the horizontal axis is the epoch. Blue lines show the value of the estimated parameter γ_i over training epochs. Since convergence was relatively fast, the horizontal axis is on a logarithmic scale for visibility. The shading highlights the variance of the trajectories before convergence.

comparison, we use the dataset first proposed in [18] and reused in [15]. The details of the equation and visualizations are given in Appendix A.4.

In Table. 2, we present a size comparison of the models along with the training time for one epoch when using the setup proposed by the authors. PAIG does not require object masks as input since it learns the segmentation via a U-Net in its pipeline. Other baselines, as well as our model for multiple objects, need masked inputs and, therefore, do not employ a segmentation block. We, therefore, also consider PAIG with masked input and without the U-Net block in our comparisons.

	Motion	Intensity	Scaling	Expected
Equation	$z^{(2)} + \gamma_1 z^{(1)} + \gamma_0 z = 0$			
γ_0	3.943 ± 0.0083	3.887 ± 0.0348	4.055 ± 0.0261	4.0016
γ_1	0.1441 ± 0.007	0.0889 ± 0.0098	0.9102 ± 0.012	0.08

Table 1. Parameter estimation accuracy. The right-most column shows the expected values. We show the mean and standard deviation of each learnable parameter in the physics block after training. The values are obtained over 7 different runs with different initializations.

	Number parameters	Time epoch (s)	Uses Decoder	Inputs Masks
PAIG [18]	5.27M	252.72	✓	✗
PAIG w/o U-Net	4.78M	80.56	✓	✓
NIRPI [15]	75.42K	0.11	✓	✓
Ours	4.19M	0.95	✗	✓

Table 2. Relevant differences between our model and the baselines.

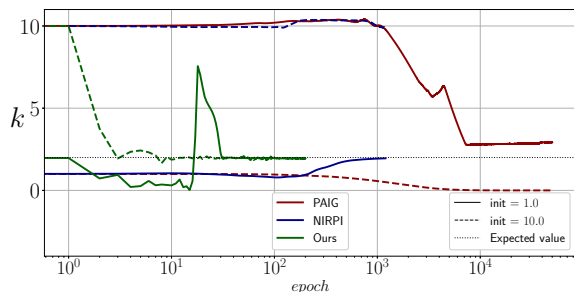


Figure 6. Robustness of the parameter estimation compared to baselines. For a fair comparison, we use the synthetic dataset created originally by the authors of the baseline papers to evaluate their models (see Appendix A.4). We plot the trajectories of the estimated parameter k during training with different initializations for our model (green) and for the two baseline models (red, blue). Dotted lines correspond to an initial value of $k = 10.0$, and solid lines to $k = 1.0$. Our model converges robustly to the ground truth value of $k = 2.0$.

Next, we empirically demonstrate the baseline’s sensitivity to initial conditions: We train each model twice in the experiment and initialize the estimated parameter k with values 1.0 and 10.0, respectively. The expected value is $k = 2$ as used in the baseline papers [15, 18]. In Figure 6, we observe that different initializations fail to converge to the correct value of k for the baselines, while our model is consistent and converges to the desired value accurately. Besides, this experiment shows our model is suitable for two dimensional problems with multiple objects.

4.6. Real-world video evaluation

For the real use cases we presented two different systems: 1. An LED light video recording with the constant brightness change over time 7, similar to the intensity problems previously studied. 2. A pendulum recording is used to validate

the model in a realistic version of the synthetic dataset. For training these models, no masks were needed in comparison to baselines [15, 18].

For an LED recording with constant change of brightness over time 7 shows that the model performs accurately (model predictions in blue) when compared with the ground truth intensity values manually extracted for each frame (red). In Figure 8, we present a more realistic use case where we do not have access to the ground truth or precise manual annotations for each frame. Fortunately, the length of the string L is known to be 120 cm (string length is not visible in the video). The task in this experiment is to learn the value of L . Quantitatively, in Figure 8a, the model can reliably estimate the value of the length parameter L . Besides, in the latent space Figure 8b, we can see that the model can accurately predict the natural damped oscillations of the pendulum.

5. Discussion and Limitations

We present a novel method to perform physical parameter estimation of governing equations. While previous methods in literature do not study phenomena other than motion, we go beyond motion and include a variety of dynamical systems.

We avoid frame prediction, which is a challenging problem but can be used for further visualization. However, this requires a decoder that needs to be designed based on the particular system. A general transformation-agnostic decoder might fail in proper reconstructions. Since our approach does not require decoders, it is applicable to different dynamical systems.

In addition, we examine latent space predictions directly. In contrast, state-of-the-art models do not discuss the accuracy of predicted dynamics compared to the real dynamics [15, 18, 20], but mainly report the frame reconstruction

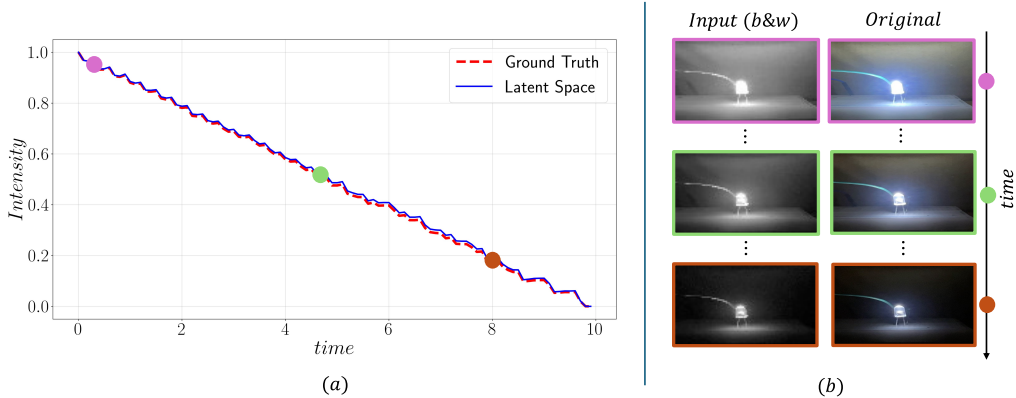


Figure 7. Estimating dynamics from a real-world linear intensity change video. **(a)** The estimated dynamics from the model (Latent Space) are compared with a fitted line and the manually extracted ground truth; the plot shows three dots where example frames of the video inputs are shown in **(b)**. **(b)** Examples of the video showing the original frames and the resized input used in the grey scale where no masks are needed. The plot in **(a)** shows that the latent space can accurately estimate the intensity, capturing the global behaviour over time and following the indicated dynamics on a real video.

Equation	Parameter	Expected (m)	Estimated (m)
$\theta^{(2)} = -\zeta\theta^{(1)} - \frac{g}{L}\sin(\theta)$	String length (L)	1.20	1.22

(a)

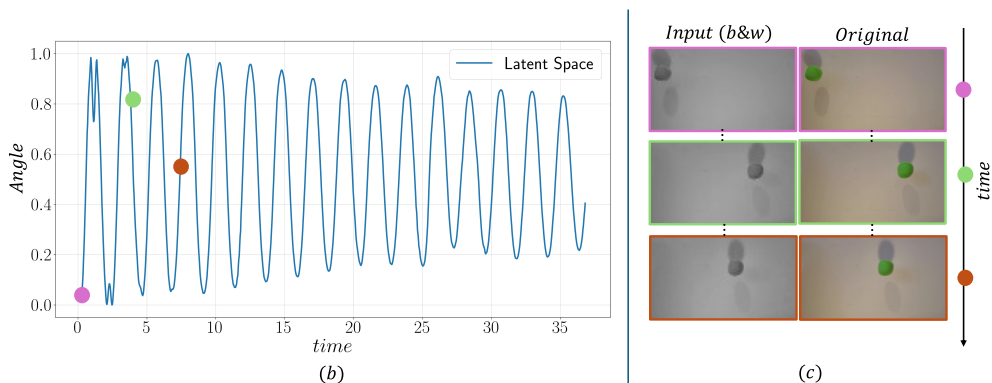


Figure 8. Real-world pendulum recording parameter estimation. **(a)** The angle θ is the latent variable. Damping factor ζ and the string length L are learned. **(b)** Extracted dynamics by the model. **(c)** Gray scale input and the original frame from the dataset, related to time in plot **(b)** using the coloured dots. Our model can estimate the parameter L with only a 0.02 m error.

accuracy. However, when the main objective is parameter estimation, reconstruction is simply a tool to define the unsupervised loss, and therefore, the latent space should be analysed closely.

Our model does not distinguish the absolute scale of the variable state, which means the model does not have the means to know that the pendulum goes from $[-90^\circ, 90^\circ]$. Yet, thanks to the loss function, the model solves its own metric, ensuring assumptions made in section 3. Baselines implicitly or explicitly do this normalization using the spatial transform, forcing the prediction to be in the pixel metric; instead, all our dynamics depend on the prior distribution assumed by KL-divergence.

Baseline methods are sensitive to the initial value of the

parameters γ . In our method, we also observed that small learning rates with high initial parameters can lead to a local minimum. Therefore, we enforce variance in the learning rate depending on the initial values of the parameters (as explained in Sec. 3, which allow for wider search spaces. Finally, our successful parameter estimation without masks on a real-world video (see Sec. 4.6) is an improvement over the baselines.

Limitations We used continuous, autonomous differential equations. However, some systems, such as fluids, are described with more complex differential equations. In addition, we need to guarantee that Eq. 8 can be differentiated. Because of the previous reasons, the research in this solution

has yet to be explored with an extension of the experiments and more complex use cases, which might include combining dynamics or multiple entities in a scene with independent dynamics.

Due to discretization, performance may vary; for example, small changes in dynamics in the scale dataset were challenging to study because of the resolution of the images.

We avoid mask prediction for the objects in video (see Sec. 4.1). In realistic settings with complex backgrounds, object masks are not necessary as input to train, as real-world experiments showed in section 4.6, while baselines require such masks [15, 18]. However, when the system involves multiple objects interacting, we need to use masks as well, as shown in experiment 4.5. While learning the masks is an interesting solution proposed in [16, 18], their method highly depends on the spatial transformer constrained to roto-translation problems.

References

- [1] Claire Adam-Bourdarios, Glen Cowan, Cecile Germain-Renaud, Isabelle Guyon, Balázs Kégl, and David Rousseau. The higgs machine learning challenge. In *Journal of Physics: Conference Series*, page 072015. IOP Publishing, 2015. 2
- [2] Mary P Anderson, W Woessner, and Randall J Hunt. Chapter 9-model calibration: assessing performance. *Applied ground-water modeling*, pages 375–441, 2015. 1
- [3] Martin Asenov, Michael Burke, Daniel Angelov, Todor Davchev, Kartic Subr, and Subramanian Ramamoorthy. Vid2param: Modeling of dynamics parameters from video. *IEEE Robotics and Automation Letters*, 5(2):414–421, 2019. 2
- [4] Nicholas M Ball and Robert J Brunner. Data mining and machine learning in astronomy. *International Journal of Modern Physics D*, 19(07):1049–1106, 2010. 2
- [5] Peter Battaglia, Razvan Pascanu, Matthew Lai, Danilo Jimenez Rezende, et al. Interaction networks for learning about objects, relations and physics. *Advances in neural information processing systems*, 29, 2016. 2
- [6] Steven L Brunton, Joshua L Proctor, and J Nathan Kutz. Discovering governing equations from data by sparse identification of nonlinear dynamical systems. *Proceedings of the national academy of sciences*, 113(15):3932–3937, 2016. 1, 2
- [7] Kathleen Champion, Bethany Lusch, J Nathan Kutz, and Steven L Brunton. Data-driven discovery of coordinates and governing equations. *Proceedings of the National Academy of Sciences*, 116(45):22445–22451, 2019. 1, 2
- [8] Miles Cranmer, Sam Greydanus, Stephan Hoyer, Peter Battaglia, David Spergel, and Shirley Ho. Lagrangian neural networks. *arXiv preprint arXiv:2003.04630*, 2020. 2
- [9] Filipe de Avila Belbute-Peres, Kevin Smith, Kelsey Allen, Josh Tenenbaum, and J Zico Kolter. End-to-end differentiable physics for learning and control. *Advances in neural information processing systems*, 31, 2018. 2, 5
- [10] Katerina Fragkiadaki, Pulkit Agrawal, Sergey Levine, and Jitendra Malik. Learning visual predictive models of physics for playing billiards. *arXiv preprint arXiv:1511.07404*, 2015. 2
- [11] Han Gao, Matthew J Zahr, and Jian-Xun Wang. Physics-informed graph neural galerkin networks: A unified framework for solving pde-governed forward and inverse problems. *Computer Methods in Applied Mechanics and Engineering*, 390:114502, 2022. 2
- [12] Craig Gin, Bethany Lusch, Steven L Brunton, and J Nathan Kutz. Deep learning models for global coordinate transformations that linearise pdes. *European Journal of Applied Mathematics*, 32(3):515–539, 2021. 2
- [13] Vincent Le Guen and Nicolas Thome. Disentangling physical dynamics from unknown factors for unsupervised video prediction. In *Proceedings of the IEEE/CVF conference on computer vision and pattern recognition*, pages 11474–11484, 2020. 2
- [14] Ryan N Gutenkunst, Joshua J Waterfall, Fergal P Casey, Kevin S Brown, Christopher R Myers, and James P Sethna. Universally sloppy parameter sensitivities in systems biology models. *PLoS computational biology*, 3(10):e189, 2007. 1
- [15] Florian Hofherr, Lukas Koestler, Florian Bernard, and Daniel Cremers. Neural implicit representations for physical parameter inference from a single video. In *Proceedings of the IEEE/CVF Winter Conference on Applications of Computer Vision*, pages 2093–2103, 2023. 1, 2, 3, 6, 7, 9, 11
- [16] Jun-Ting Hsieh, Bingbin Liu, De-An Huang, Li F Fei-Fei, and Juan Carlos Niebles. Learning to decompose and disentangle representations for video prediction. *Advances in neural information processing systems*, 31, 2018. 2, 3, 9
- [17] Raban Iten, Tony Metger, Henrik Wilming, Lidia Del Rio, and Renato Renner. Discovering physical concepts with neural networks. *Physical review letters*, 124(1):010508, 2020. 1, 2
- [18] Miguel Jaques, Michael Burke, and Timothy Hospedales. Physics-as-inverse-graphics: Unsupervised physical parameter estimation from video. In *International Conference on Learning Representations*, 2020. 1, 2, 3, 5, 6, 7, 9, 11
- [19] Navami Kairanda, Edith Tretschk, Mohamed Elgharib, Christian Theobalt, and Vladislav Golyanik. f-sft: Shape-from-template with a physics-based deformation model. In *Proceedings of the IEEE/CVF Conference on Computer Vision and Pattern Recognition*, pages 3948–3958, 2022. 2
- [20] Rama Kandukuri, Jan Achterhold, Michael Moeller, and Joerg Stueckler. Learning to identify physical parameters from video using differentiable physics. In *DAGM German conference on pattern recognition*, pages 44–57. Springer, 2020. 2, 7
- [21] George Em Karniadakis, Ioannis G Kevrekidis, Lu Lu, Paris Perdikaris, Sifan Wang, and Liu Yang. Physics-informed machine learning. *Nature Reviews Physics*, 3(6):422–440, 2021. 2
- [22] Diederik P Kingma and Jimmy Ba. Adam: A method for stochastic optimization. *arXiv preprint arXiv:1412.6980*, 2014. 10
- [23] Diederik P Kingma and Max Welling. Auto-encoding variational bayes. *arXiv preprint arXiv:1312.6114*, 2013. 2, 4
- [24] Jannik Kossen, Karl Stelzner, Marcel Hussing, Claas Voelcker, and Kristian Kersting. Structured object-aware physics

- prediction for video modeling and planning. *arXiv preprint arXiv:1910.02425*, 2019. 2
- [25] Attila Lengyel, Sourav Garg, Michael Milford, and Jan C van Gemert. Zero-shot day-night domain adaptation with a physics prior. In *Proceedings of the IEEE/CVF International Conference on Computer Vision*, pages 4399–4409, 2021. 2
- [26] Maxwell W Libbrecht and William Stafford Noble. Machine learning applications in genetics and genomics. *Nature Reviews Genetics*, 16(6):321–332, 2015. 2
- [27] Michael Lutter, Christian Ritter, and Jan Peters. Deep lagrangian networks: Using physics as model prior for deep learning. *arXiv preprint arXiv:1907.04490*, 2019. 2
- [28] Erik Meijering, Anne E Carpenter, Hanchuan Peng, Fred A Hamprecht, and Jean-Christophe Olivo-Marin. Imagining the future of bioimage analysis. *Nature biotechnology*, 34(12):1250–1255, 2016. 2
- [29] Zeng Meng, Qiaochu Qian, Mengqiang Xu, Bo Yu, Ali Rıza Yıldız, and Seyedali Mirjalili. Pinn-form: A new physics-informed neural network for reliability analysis with partial differential equation. *Computer Methods in Applied Mechanics and Engineering*, 414:116172, 2023. 2
- [30] Jaques Miguel. Physics-as-inverse-graphics. <https://github.com/seuqaj114/paig>, 2019. 6
- [31] M. Raissi, P. Perdikaris, and G.E. Karniadakis. Physics-informed neural networks: A deep learning framework for solving forward and inverse problems involving nonlinear partial differential equations. *Journal of Computational Physics*, 378:686–707, 2019. 2
- [32] Michael Schmidt and Hod Lipson. Distilling free-form natural laws from experimental data. *science*, 324(5923):81–85, 2009. 1
- [33] Naoya Takeishi and Alexandros Kalousis. Physics-integrated variational autoencoders for robust and interpretable generative modeling. *Advances in Neural Information Processing Systems*, 34:14809–14821, 2021. 2
- [34] Peter Toth, Danilo Jimenez Rezende, Andrew Jaegle, Sébastien Racanière, Aleksandar Botev, and Irina Higgins. Hamiltonian generative networks. *arXiv preprint arXiv:1909.13789*, 2019. 2
- [35] Gaël Varoquaux and Veronika Cheplygina. Machine learning for medical imaging: methodological failures and recommendations for the future. *NPJ digital medicine*, 5(1):48, 2022. 2
- [36] Petar Veličković, Matko Bošnjak, Thomas Kipf, Alexander Lerchner, Raia Hadsell, Razvan Pascanu, and Charles Blundell. Reasoning-modulated representations. In *Learning on Graphs Conference*, pages 50–1. PMLR, 2022. 2, 5
- [37] Nicholas Watters, Daniel Zoran, Theophane Weber, Peter Battaglia, Razvan Pascanu, and Andrea Tacchetti. Visual interaction networks: Learning a physics simulator from video. *Advances in neural information processing systems*, 30, 2017. 2, 5
- [38] Sebastian Weiss, Robert Maier, Daniel Cremers, Rudiger Westermann, and Nils Thuerey. Correspondence-free material reconstruction using sparse surface constraints. In *Proceedings of the IEEE/CVF Conference on Computer Vision and Pattern Recognition*, pages 4686–4695, 2020. 2, 3
- [39] Jiajun Wu, Ilker Yildirim, Joseph J Lim, Bill Freeman, and Josh Tenenbaum. Galileo: Perceiving physical object properties by integrating a physics engine with deep learning. *Advances in neural information processing systems*, 28, 2015. 2
- [40] Jiajun Wu, Erika Lu, Pushmeet Kohli, Bill Freeman, and Josh Tenenbaum. Learning to see physics via visual de-animation. In *Advances in Neural Information Processing Systems*. Curran Associates, Inc., 2017. 2
- [41] Tsung-Yen Yang, Justinian Rosca, Karthik Narasimhan, and Peter J Ramadge. Learning physics constrained dynamics using autoencoders. *Advances in Neural Information Processing Systems*, 35:17157–17172, 2022. 5
- [42] David Zheng, Vinson Luo, Jiajun Wu, and Joshua B Tenenbaum. Unsupervised learning of latent physical properties using perception-prediction networks. *arXiv preprint arXiv:1807.09244*, 2018. 2, 5
- [43] Yaofeng Desmond Zhong and Naomi Leonard. Unsupervised learning of lagrangian dynamics from images for prediction and control. In *Advances in Neural Information Processing Systems*, pages 10741–10752. Curran Associates, Inc., 2020. 2

A. Appendix / supplemental material

A.1. Dataset Dimensionality

Each uses an image size of (50×50) pixels, and the simulated dynamics are the same for the three datasets (Eq. 2) normalized with respect to the image size and maximum pixel intensity. Each dataset consists of 500 training samples with 20 frames, with a final numerical dimensionality of $(samples \times frames \times \#channels \times width \times height) = (500 \times 20 \times 1 \times 50 \times 50)$.

A.2. Training Hyperparameters

The experiments and baselines were executed on a GPU NVIDIA 3080. For our model, implemented in PyTorch, the encoder was trained using the Adam optimizer [22] with a learning rate of $1 \times e^{-2}$ and the default weight initialization for MLP layers.

A.3. Simulation Details

Here we discuss the details of the dynamics simulation of the experiments in section 4.3. The equation 2 represents and harmonic oscillator with close solution:

$$z(t) = Ae^{-\zeta t} \cos(\omega t + \phi) \quad (14)$$

Where $\omega = 2$ is the frequency we used for simulation and $\zeta = 0.04$ the damping factor. this parameter relates to γ as follows:

$$\gamma_0 = \omega^2 + \zeta^2 = 4.0016 \quad (15)$$

$$\gamma_1 = 2\zeta = 0.08 \quad (16)$$



Figure 9. **Dataset baseline.** It shows the evolution of the spring dynamical system of two MNIST digits over a static CIFAR10 background. Figure edited from [18]

A.4. Baseline Dataset

In this section, we describe the dataset used to compare the baselines. Both baselines were tested in the dataset published by [18] and also used in [15], the equations of motion used for each system are presented in Eq. 17

$$\vec{F}_{i,j} = -k(\vec{p}_i - \vec{p}_j) - l \frac{\vec{p}_i - \vec{p}_j}{|\vec{p}_i - \vec{p}_j|} \quad (17)$$